Preliminary geochemical characterization of the Mts. Simbruini karst aquifer (Central Italy)

Marianna Cangemi[1], Massimo Ranaldi[2,*], Maria Luisa Carapezza[2], Marco Vinci[3] and Paolo Madonia[4]

[1] Dipartimento di Science della Terra e del Mare, Università degli Studi di Palermo, Palermo, Italy

[2] Istituto Nazionale di Geofisica e Vulcanologia, Sezione Roma 1, Roma, Italy

[3] GeoStudioVinci, Guidonia Montecelio, Roma, Italy

[4] Istituto Nazionale di Geofisica e Vulcanologia, Sezione Roma 2, Roma, Italy

Abstract

Mts. Simbruini karst aquifer feeds important springs whose capture contributes to the water supply of Rome City. To improve the geochemical characterization of this aquifer, we analyzed 36 groundwater samples, 29 from springs and 7 from shallow wells, collected in 1996 and 2019. Atomic adsorption spectroscopy, titration, ionic chromatography and mass spectrometry were the used analytical methods. Groundwater is bicarbonate alkaline-earth type and HCO_3^- dominance confirms that the aquifer is hosted in carbonate rocks. Total alkalinity vs. cations plot indicates that CO_2 driven weathering controls the water chemistry. The probability plots of HCO_3^-, cations and Ca^{2+} $+Mg^{2+}$ indicate four groundwater populations with the less represented one (9 samples) characterized by the highest PCO_2 values (> 0.3 atm). Most anomalous values of the dissolved PCO_2 are from springs located near the center of the studied area. Four samples have negative values of $\delta^{13}C_{CO_2}$ (about -22‰ vs. PDB), indicating its organic origin, but two other samples have positive values (1.6 and 2.6 ‰ vs. PDB), similar to those observed in the CO_2 of deep origin discharged at the close Colli Albani volcano. Therefore, geochemical evidence indicates that the Mts. Simbruini aquifer is locally affected by the input of deep originated CO_2, likely rising up along fractures, interacting with a recharge of meteoric origin, as evidenced by its δ^2H and $\delta^{18}O$ isotopic signatures.

Keywords: Water resources; Groundwater processes; Chemistry of waters; Hydrological processes: interaction, transport, dynamics; Fluid Geochemistry.

1. Introduction

Because of the large diffusion worldwide of outcropping limestone rocks, karst aquifers are amongst the most important suppliers of drinkable water [Stevanovic, 2015]. Karst aquifers represent about the 40% of the supply of drinkable water in the Mediterranean in general, and in Italy in particular. The 90% of water distributed by the metropolitan aquifer of Rome is of karst origin [Società Speleologica Italiana, 2002].

Many of these are located in the Aniene river valley, between Mts. Simbruini and Mts. Ruffi (Figure 1). The main aquifer of the area is hosted within the Simbruini calcareous rocks, particularly where important karst phenomena

Marianna Cangemi et al.

developed, increasing significantly the rock permeability [Vinci, 1998]. The hydrogeology of this area has been described in detail in the unpublished thesis of Vinci [1998], who reported also some chemical analyses of the groundwater, but without developing a detailed geochemical study, of great importance for the characterization and management of the huge aquifers of Mts. Simbruini. With the aim of completing and extending these first data, we carried out a more detailed geochemical study of the area, collecting and analyzing in May 2019 six new samples from springs and compared the results with the unpublished data collected in May 1996 [Vinci, 1998]. In doing this, we followed the same approach used by Madonia et al. [2020] for describing the characteristics of the main karst aquifer of Central Italy, of which study the present article represents the completion.
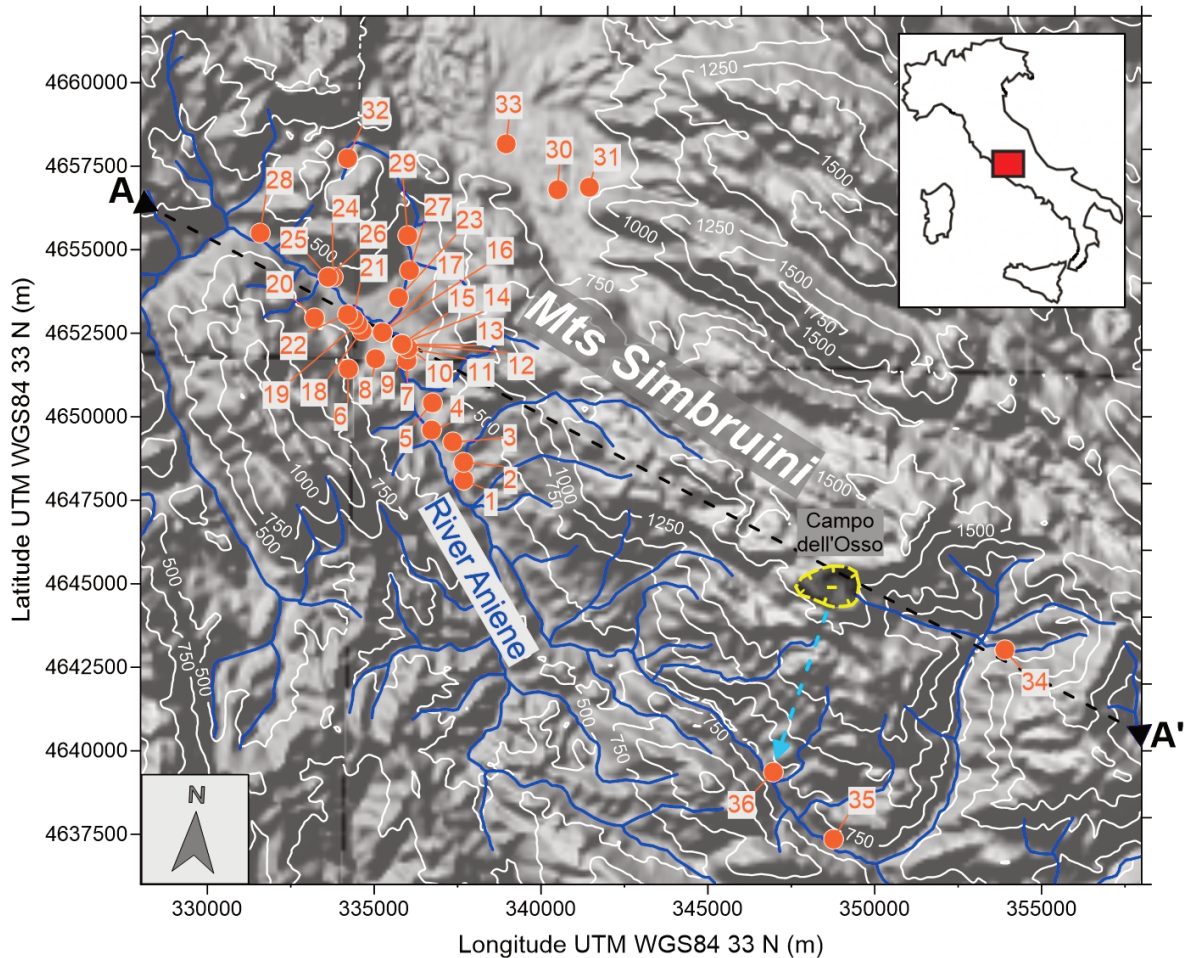
Figure 1. Location of the studied area (inset in the upper right) and shaded relief map reporting position of sampling points (orange circles), elevations (white lines, contour interval 250 m) and the hydrographic network of the River Aniene (blue lines). Trace (A-A', dashed black line) of the hydrogeologic profile of Figure 3 and the endoreic karst plateau of Campo dell'Osso (in yellow) are also shown. The cyan dashed line indicates the fast karst hydrogeologic circuit connecting the Campo dell'Osso plateau with the resurgence of the "Inferniglio" (spring no. 36).

Some of the groundwaters contain free CO_2 bubbles [Vinci, 1998] and to investigate the CO_2 abundance and origin, we calculated the PCO_2 in 36 samples and carried out $\delta^{13}C$ isotopic analyses on the six 2019 groundwater samples.

Although all groundwaters are from a calcareous aquifer, minor but significant difference exist in their geochemical characteristics, which are mainly governed by water-rock interaction, and CO_2-driven weathering.

In this paper we describe the geochemistry of the Simbruini karst aquifer and discuss the isotopic evidence that suggest the presence of local inputs of deep originated CO_2.

2. Geological and hydrogeological outlines

The study area is located in Central Italy, in the western part of Latium-Abruzzi Apennines, whose geodynamic evolution involves sedimentary complexes belonging to two contiguous paleogeographic domains. These are represented by the carbonatic platform series of Latium-Abruzzi (Upper Trias-Upper Cretaceous) and the Miocene Sabina transitional series [Fabbi, 2016].

In particular, the study area is located on the Simbruini-Ernici ridge belonging to the Latium-Abruzzi carbonate platform (Figures 1 and 2). This ridge is a big NE dipping monocline, overrun on the Upper Miocene Latium-Abruzzi siliciclastic deposits [Fabbri, 2016]. The Simbruini-Ernici ridge consists of three partially overlapped tectonic units. The most internal one consists mainly of ~40° NE dipping Cretaceous calcareous sequences, overrun above the intermediate tectonic unit which is made of a monocline of dolomitic rocks (Dogger-Malm), with 45° NNE dipping. The external tectonic unit also consists mostly of a monocline of NNE dipping Cretaceous calcareous strata, which generate reverse faults at its front [Vinci, 1998].

The area is characterized by the presence of eight hydrogeological complexes (Figure 2) distinguished on the basis of the Aquifer Potential Evaluation (APE), i.e. their average permeability and water infiltration efficiency [Capelli et al., 2012]. The alluvial deposits complex is the most recent (Holocene), it has a low to medium-high APE and a thickness of a few meters to more than one hundred meters. The thickest deposits contain multilayer aquifers of regional importance. The detrital deposits complex (Pleistocene-Holocene) has a medium-high APE and a thickness up to a few tens of meters. It does not contain any significant aquifer apart from seasonal perched ones. The complex of marly arenaceous flysch (middle - upper Miocene) has a medium-low APE. It is some hundred meters thick without any water circulation of regional importance. The marly-limestone basin complex (Eocene-Miocene) has medium-low APE, with a maximum thickness of some hundred meters. This complex represents the hydraulic seal because of its high marl component. The marly-limestone platform complex (Upper Cretaceous-Miocene) has a medium-high APE, with thickness up to hundred meters. Limestones favour the recharge of the regional aquifers whereas the marly component sustains modest local aquifers. The marly-clayey flysch complex (Upper Cretaceous -Oligocene) has a very low APE, thickness up to 1000 m and does not host any aquifer. The most important hydrogeological complex is the platform limestone complex (Middle Cretaceous-Upper Lias) with a very high APE and a thickness ranging from a few hundred meters to 1500 m. It hosts large aquifers feeding the main springs of Lazio Region. The basal dolomitic complex (Trias–Lower Lias) has a medium-low APE and thickness up to hundreds of meters. Its permeability is lower than that of the platform limestones and therefore it plays the role of base aquitard of the underground circulation.

In summary, the Mts. Simbruini form a large NW-SE hydrogeological complex, consisting of a ~4000 m thick succession of calcareous rocks, surrounded at its base by low-permeability siliciclastic deposits, which insulate it hydraulically from the adjacent groundwater circulation systems [Vinci, 1998]. The carbonate rocks have a marked secondary permeability that favored the development of shallow and deep karst phenomena, allowing the formation of an important base aquifer, mainly flowing north-eastward and whose aquiclude is seated on the low permeability dolomites. Many springs spill out at the contact between the base dolomitic succession and the overlying calcareous rocks, presently almost totally used for the Marcio aqueduct of Rome city. A schematic hydrogeological cross section, whose trace (A-A') is reported in Figure 2 is illustrated in Figure 3.

3. Materials and Methods

Data of the present work are related to a previous unpublished study carried out in the second half of 1990s', integrated by new samples collected in May 2019. The first includes 30 samples, 23 of which from springs and 7 from wells [Vinci, 1998]. The second campaign was carried out in May 2019, far from the last heavy rains for avoiding the collection of samples perturbed by shallow, fast groundwater circulation, and includes 6 spring samples. Location of sampling sites is shown in Figure 1. Electric conductivity, pH and Eh were measured in the field using electrochemical sensors. Water samples of the 1996 campaign were first filtered using 0.45 μm Millipore MF filter and then collected in 2L LD-PE (low-density polyethylene) bottles, acidifying with HCl to ca. pH 2 the aliquot destined to cation determination, which was carried out by atomic absorption spectroscopy.

SO_4^{2-} and NO_3^- were determined by spectroscopy (Perkin Elmer MKIII), whereas chlorine content was determined by tritration. The May 2019 water samples were analysed at the lab facilities of Istituto Nazionale di Geofisica e
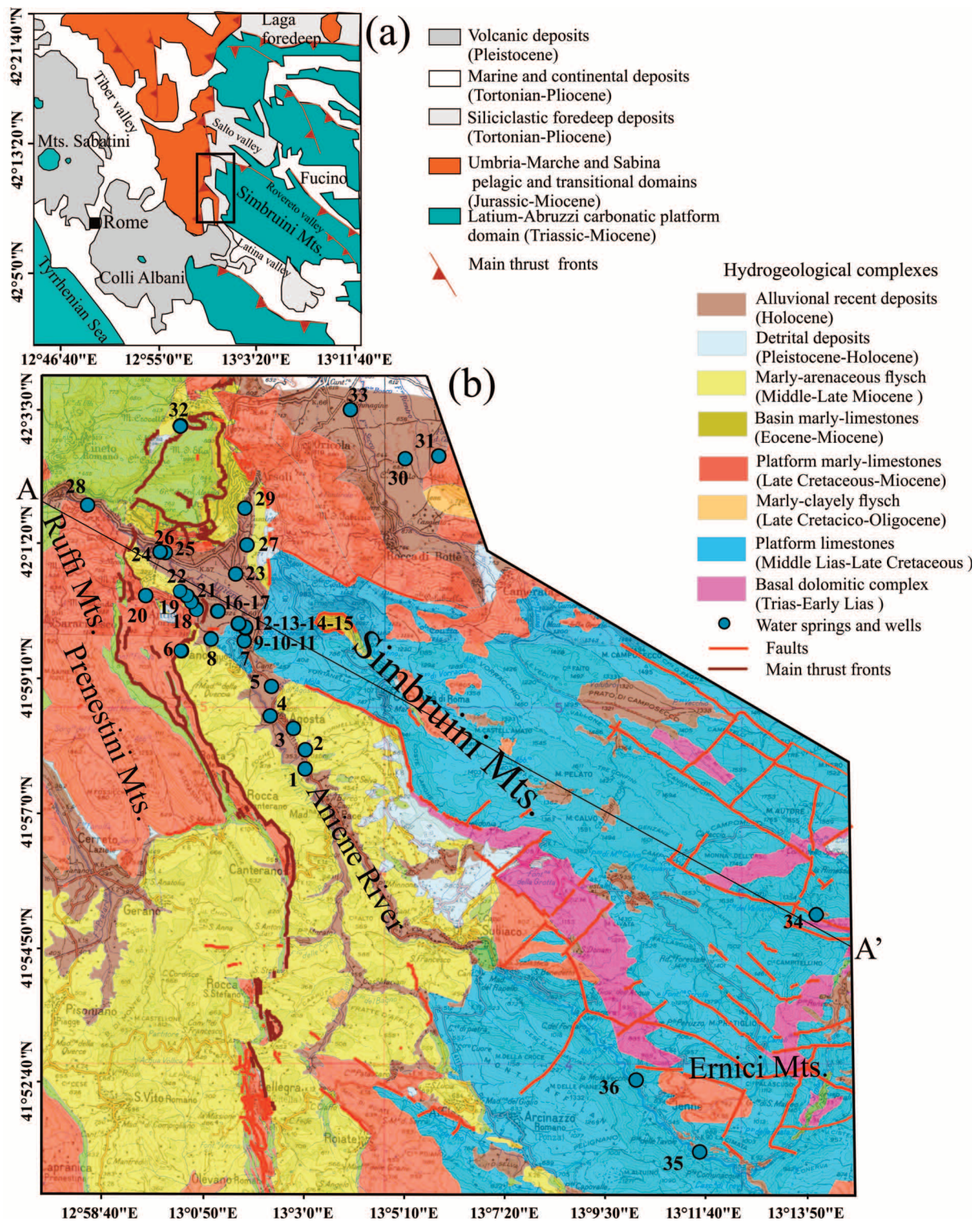
Figure 2. (a) Geology of Central Italy (modified after Carminati et al. [2014]). Black rectangle indicates the study area; (b) Schematic hydrogeological map of the Simbruini Mts. (modified after Capelli et al. [2012]). A-A' is the trace line of the cross-section of Figure 3. Base map Latium Regional Technical Cartography (CTR), scale 1:100.000 geographical coordinates in WGS 84.

Vulcanologia (INGV), Sezione di Palermo. Samples used for the determination of dissolved major and trace elements, were first filtered using 0.45 μm Millipore MF filter and then collected in LD-PE bottles for major element analyses, acidifying with HNO_3^- to ca. pH 2 the aliquot destined to cation determination. Untreated aliquots were collected for isotopic and alkalinity determinations, made via tritration with HCl (0.1 N). Major ions were determined by ionic chromatography, using Dionex columns AS14 and CS12 for anions and cations respectively.

We used the PHREEQC software [Parkhurst and Appelo, 2020] for calculating saturation indexes of calcite and partial pressure CO_2 (PCO_2), adopting the LLNL database. Starting from anaylitcal data, we calculated the PCO_2 in the sampled waters from pH and alkalinity using the constants K_H and K_1 once the temperature is known, following the procedure reported by Cangemi et al. [2020]. The calculated PCO_2 values were plotted in a contour map using Golden Software Surfer (release 13), with the kriging interpolation algorithm.

Samples for analyses of dissolved gases and $\delta^{13}C$ of Total Dissolved Inorganic Carbon (TDIC) were collected in glass bottles, hermetically capped with a crimper.

The determination of δ^2H [Kracht, et al., 2016] and $\delta^{18}O$ [Andreas and Hairigh, 2008] of water was performed by using a Thermo Delta Plus XP IRMS, coupled with an online pyrolysis system (TC/EA Thermal Conversion Elemental Analyzer) for ^2H /^1H ratio, and by CO_2-water equilibration technique using a Thermo Delta V Plus instrument, equipped with a Gas Bench II, for ^{18}O/^{16}O ratio. The results were reported in d‰ versus the V-SMOW standard, with a precision better than ± 1‰ for d^2H and ± 0.1‰ for $\delta^{18}O$. The isotopic composition of the Total Dissolved Inorganic Carbon ($\delta^{13}C_{TDIC}$) was determined with the method proposed by Capasso et al. [2005], using a Thermo Delta V Plus IRMS coupled with an on-line gas preparation system Gas Bench II. The results were reported in δ‰ versus the V-PDB standard, with a precision better than ± 0.1‰. The correspondent values of $\delta^{13}C$ of CO_2 in equilibrium with TDIC, used in graphical representations, were calculated using the formula proposed by Zhang et al. [1995].

The chemical composition of the dissolved gasses (CH_4 and CO_2) was determined according to the procedure by Capasso and Inguaggiato [1998]; this method is based on the equilibrium between the liquid and the gas phases in the headspace of the bottles. We used an Agilent (Santa Clara, CA, USA) 78909 GC instrument, with Ar as gas carrier and TCD-FID as detectors; analytical accuracy was better than 5%.
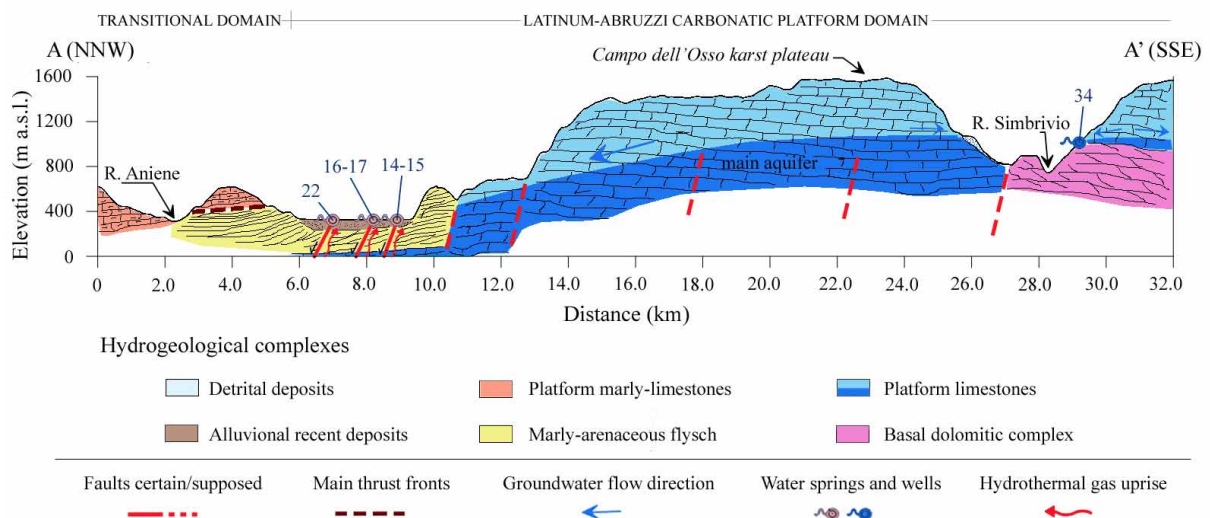

Figure 3. Schematic hydrogeological profile of the studied area (trace shown in Figure 1 and 2).

4. Results and Discussion

4.1 Physical, Chemical and Isotopic Characteristics of Groundwater

Field data are reported in Table 1. Groundwater samples are characterized by an average electrical conductivity (E.C.) of ~ 925 µS cm^{-1}, with a minimum of 340 µS cm^{-1} (INF spring no. 36) and a maximum of 2380 µScm^{-1} recorded at no. 13 spring. The average value of pH is ~ 6.95, with a minimum of 6.04 and a maximum of 8.30. Chemical data are reported in Table 2; Table 3 shows the additional data (isotopic compositions and Eh) related to the 2019 field campaign. The most abundant cation is Ca^{2+} (mean concentration 196 mg L^{-1}), followed by Mg^{2+} (29.9 mg L^{-1}) and to a minor extent, by Na$^+$ and K$^+$ (7.68 and 2.05 mg L^{-1}, respectively).

Id.	Lon.	Lat.	Elevation (m)	Date	T (°C)	pH	E.C. (µS cm^{-1})	Source*
1w	13.0412	41.9682	335	May 1996	11.8	6.83	850	2
2	13.0410	41.9731	360	May 1996	13.5	7.72	350	2
3	13.0369	41.9784	350	May 1996	12.3	7.14	575	2
4	13.0289	41.9814	328	May 1996	11.8	7.14	560	2
5	13.0291	41.9888	330	May 1996	10.1	7.08	505	2
6	12.9984	41.9974	550	May 1996	12.2	8.3	385	2
7	13.0195	42.0002	328	May 1996	12.3	6.98	685	2
8	13.0082	42.0004	330	May 1996	11.5	7.15	600	2
9	13.0199	42.0034	328	May 1996	14.5	6.29	1587	2
10	13.0198	42.0034	328	May 1996	13.6	6.4	1329	2
11	13.0198	42.0036	328	May 1996	14.1	6.42	1372	2
12	13.0174	42.0044	328	May 1996	13.2	6.26	1935	2
13	13.0176	42.0045	328	May 1996	17.2	6.11	2380	2
14	13.0175	42.0045	328	May 1996	12.4	6.53	985	2
15	13.0175	42.0045	326	May 2019	17.1	6.04	2031	1
16	13.0103	42.0075	324	May 1996	15.5	6.3	2110	2
17	13.0104	42.0075	323	May 2019	16.6	6.35	1990	1
18	13.0030	42.0079	325	May 1996	12.2	6.74	846	2
19	13.0014	42.0097	327	May 1996	12.9	6.63	960	2
20	12.9859	42.0110	500	May 1996	12	7.75	408	2
21	12.9999	42.0111	330	May 1996	13.2	6.5	1080	2
22	12.9977	42.0122	327	May 1996	13	6.54	1072	2
23	13.0161	42.0170	329	May 2019	11.5	7.51	577	1
24w	12.9921	42.0220	345	May 1996	12.6	7.01	732	2
25	12.9904	42.0221	328	May 1996	11.5	6.86	710	2
26	12.9904	42.0221	328	May 1996	11	6.94	641	2
27w	13.0197	42.0244	347	May 1996	12.2	7.06	615	2
28w	12.9654	42.0335	320	May 1996	12.9	6.3	1715	2
29	13.0187	42.0337	355	May 1996	11.4	7.07	622	2
30w	13.0726	42.0471	686	May 1996	13.1	7.57	450	2
31w	13.0840	42.0480	665	May 1996	13.3	7.45	438	2
32	12.9963	42.0541	700	May 1996	10.6	7.28	510	2
33w	13.0537	42.0591	620	May 1996	12.8	7.33	560	2
34	13.2378	41.9256	885	May 2019	9.7	7.47	404	1
35	13.1774	41.8737	540	May 2019	13.1	7.65	408	1
36	13.1554	41.8915	526	May 2019	9.9	7.47	340	1

Table 1. Location and field parameters of water samples.

*1: this paper; 2: after [Stevanovic, 2015]. "w" indicates that the sample is from a well; all other samples are from springs.

| Id.	Na$^+$	K$^+$	Mg^{2+}	Ca^{2+}	Cl$^-$	NO$_3^-$	SO$_4^{2-}$	HCO$_3^-$	PCO$_2$	SI calcite
1w	3.22	0.39	18.7	166	16	15.5	69.2	494	0.07	0.084
2	2.99	0.78	9.12	80.4	5.32	0.06	0.48	275	0.005	0.52
3	4.83	1.56	15.6	115	14.2	0.62	8.17	397	0.028	0.199
4	3.22	0.78	21.5	111	7.09	1.86	0.961	429	0.03	0.207
5	2.3	0.78	22.2	109	5.32	0.62	1.92	414	0.033	0.101
6	2.99	0.78	10.3	80.4	5.32	0.31	1.92	281	0.001	1.066
7	2.99	0.78	24.7	130	10.6	0.62	1.44	489	0.05	0.163
8	4.37	0.78	20.7	120	0.89	0.62	12.5	445	0.03	0.254
9	36.6	8.99	56.5	360	5.32	0.62	212	1222	0.579	0.174
10	3.45	1.56	28.7	300	5.32	0.62	23.1	1017	0.379	0.18
11	3.45	1.56	36.5	288	8.86	0	17.8	1031	0.369	0.194
12	4.6	3.13	31.4	485	8.86	0.62	21.1	1623	0.799	0.369
13	38.9	8.6	69.6	543	5.32	0.62	186	1891	1.35	0.335
14	3.45	1.17	26.6	196	5.32	0.62	10.6	732	0.205	0.019
15	4.67		124	431	11.9		20.9	1867	1.57	0.182
16	56.3	7.43	82.3	490	8.86	0.62	265	1709	0.776	0.418
17	4.51		125	409	11		18.3	1847	0.759	0.462
18	3.91	0.39	25	162	3.55	1.24	3.36	604	0.105	0.085
19	4.6	1.56	28	191	7.09	1.86	3.84	709	0.159	0.105
20	3.68	0.78	2.43	93	8.86	0.62	3.36	275	0.005	0.587
21	4.6	1.56	32.5	223	5.32	0.62	21.1	811	0.243	0.081
22	4.6	1.56	30	207	3.55	0.62	4.32	799	0.219	0.09
23	7.54		20.2	107	10.8	3.64	9.63	404	0.012	0.528
24w	5.75	2.35	25.4	136	8.86	2.48	12.5	549	0.052	0.254
25	8.28	1.17	30	117	7.09	7.44	8.65	512	0.068	0.001
26	3.22	0.78	21.5	134	7.09	0.62	8.65	512	0.056	0.134
27w	6.9	1.95	13.9	147	12.4	0.62	8.65	525	0.044	0.319
28w	2.99	0.78	21.6	411	8.86	0.62	12.5	1354	0.617	0.288
29	6.44	1.95	10.3	126	8.86	5.58	10.6	429	0.035	0.183
30w	3.91	2.74	18.7	61.9	8.86	0.62	1.92	287	0.008	0.27
31w	5.98	3.52	13.1	68.1	12.4	0.62	7.21	280	0.01	0.185
32	7.82	0.78	8.87	110	16	0	19.7	334	0.017	0.23
33w	4.37	0.39	25.5	118	12.4	12.4	8.65	440	0.02	0.435
34	2.41		15.4	76	4.04		2.69	304	0.01	0.227
35	3.45		3.74	92.6	5.48	0.98	3.05	282	0.006	0.514
36	3.24		6.83	65.1	6.29	1.58	2.42	229	0.008	0.067

Table 2. Element concentration (in mg L^{-1}), PCO$_2$ (atm) and saturation index (SI) of calcite of ground waters.
*1: this paper; 2: after [Vinci, 1998]. "w" indicates that the sample is from a well; all other samples are from springs.

In decreasing order of abundance, anions are represented by HCO$_3^-$ (mean value 716 mg L^{-1}), SO$_4^{2-}$ (mean value 28.5 mg L^{-1}), Cl$^-$ (mean value 8.14 mg L^{-1}) and NO$_3^-$ (mean value 2 mg L^{-1}). The relative abundances of the main dissolved ions classify the studied groundwater as bicarbonate alkaline-earth type, as shown in the Langelier-Ludwig diagram (Figure 4); minor contributions of Na$^+$ and K$^+$ are also evidenced. The anion ternary diagram (Figure 5a) further confirms that the quasi totality of samples falls close to the HCO$_3^-$ corner, with a trend moving toward the SO$_4$ vertex, confirming that the aquifer is mainly constituted by carbonate rocks. The cation ternary diagram (Figure 5b) indicates that, apart Ca^{2+} that represents the main cation, a variable amount of Mg^{2+} occurs in the groundwater.

Figure 6a shows the total alkalinity against the sum of cations ($\sum$cat). All samples fall close to the 1:1 line, indicating that weathering driven by CO$_2$ is the main process controlling the chemical composition of the water. Moreover, Figure 6b shows a direct relationship between Ca^{2+} +Mg^{2+} and the total alkalinity. High Ca^{2+} and Mg^{2+}

levels in groundwater are mainly recorded when the aquifers are made of carbonate rocks, pointing out that water-rock interaction is the main source of these dissolved ions. Furthermore, calculated PCO_2 vs. $Ca^{2+} + Mg^{2+}$ diagram (Figure 6c) indicates a direct relationship between these two parameters.
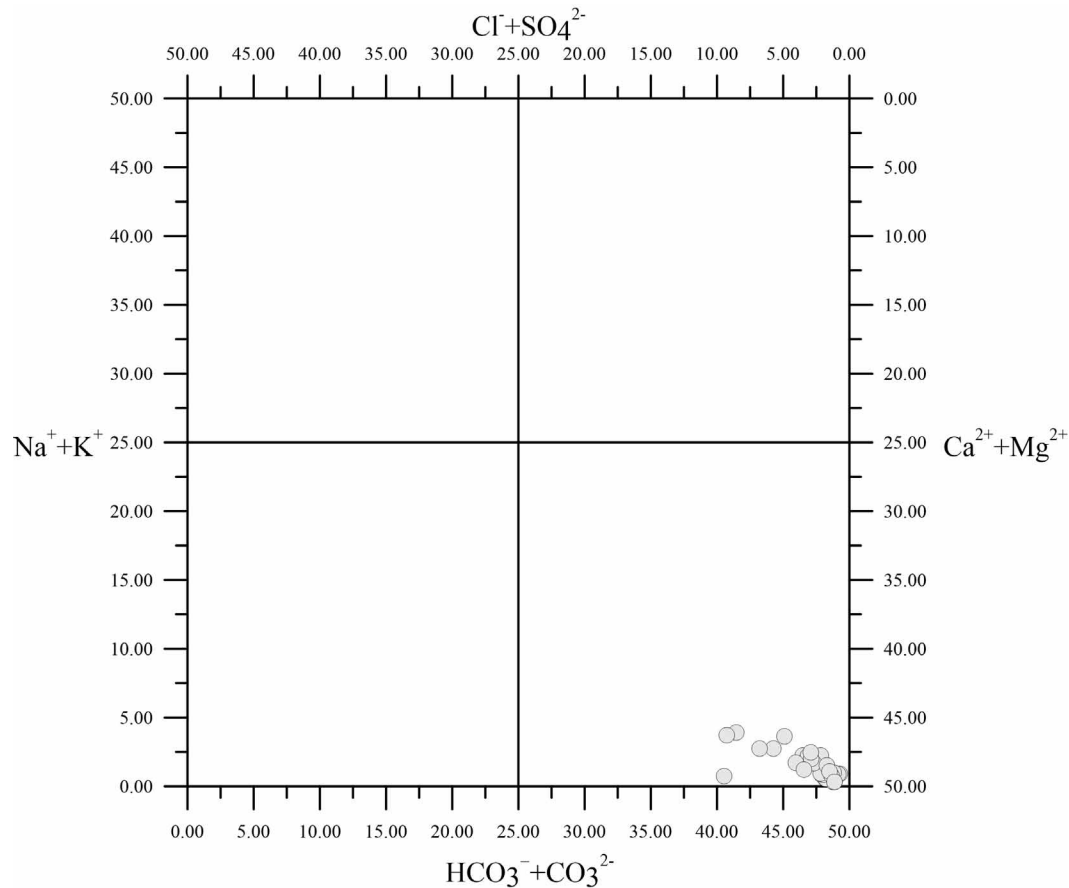
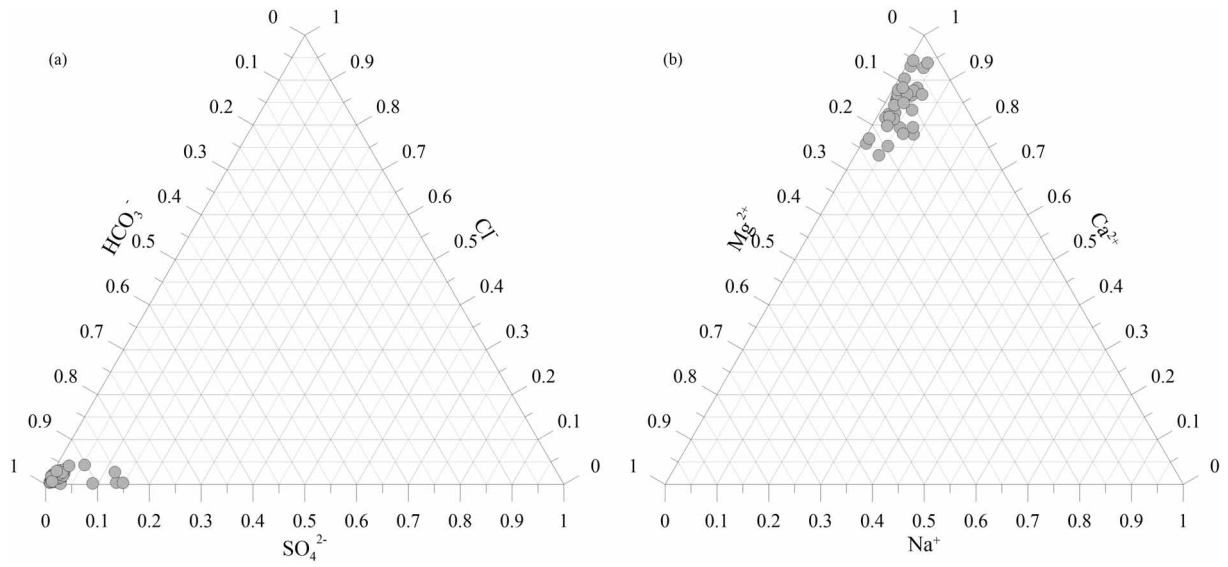**Figure 4.** Plot of Simbruini groundwaters in the Langelier-Ludwig diagram.

Saturation indexes (Figure 6d) indicate that groundwaters are at equilibrium or oversaturated with respect to calcite. Saturation indexes are not related to calculated PCO_2 when this parameter is low. Conversely, SI are directly related to PCO_2 in samples exhibiting higher carbon dioxide contents.

We used probability plots for identifying different populations of data [Sinclair, 1974]. Generally, data belonging to a single population are distributed along a straight line, so the presence of multiple straight lines with different slopes indicates the occurrence of various populations with a different origin. Probability plots of HCO_3^-, Scations and $Ca^{2+} + Mg^{2+}$ exhibit a similar distribution, with tree inflection points reflecting four populations of data (Figure 7). The first two populations include ca. 70% of the samples, ca. 28% of the samples are in population III and the remaining 2% is contained in population IV, composed of samples with the highest PCO_2 values, whose maxima are found in samples 13 and 15.

The concentration of dissolved CH_4 and CO_2 are reported in Table 3 (2019 samples). Sites 15 and 17 exhibit the highest concentrations for both species, whereas in the other samples their concentrations are 2-3 order of magnitude lower. δ^2H and $\delta^{18}O$ values range from -56.6 to -45.2 ‰ and -9.4 to -7.9 ‰ (vs V-SMOW) respectively (Table 3). These values are reported in the $\delta^{18}O$ vs δ^2H diagram of Figure 8, also showing reference data [Madonia, et al., 2020] for other karst aquifers of Central Italy and the lines representative of groundwater [Celico, et al., 1984] and rainwater [Longinelli and Selmo, 2003] for the study area, and the Global Meteoric Water Line (GMWL) [Craig, 1961]. The points fall in the area of groundwater by [2015], being shifted upward with respect to the rainwater line of [Longinelli and Selmo, 2003].
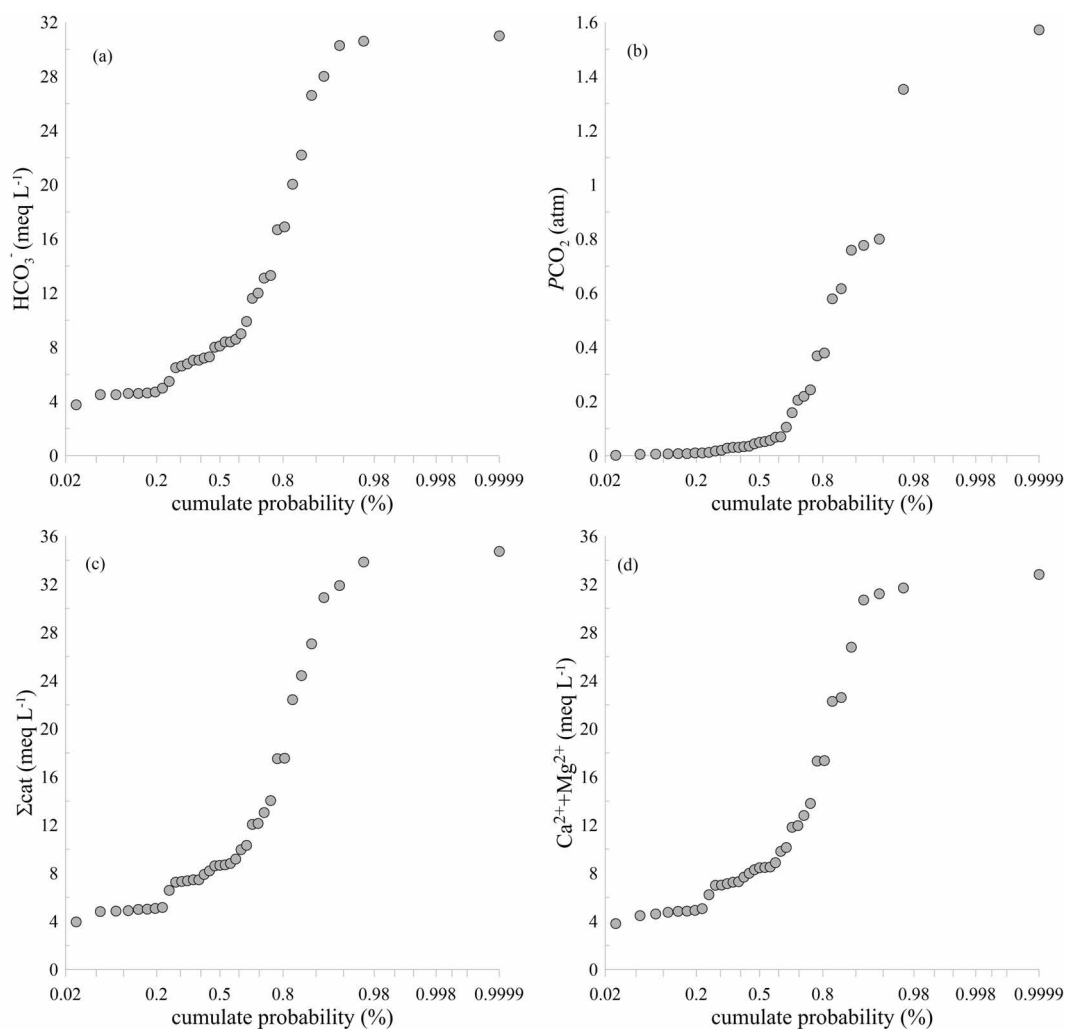
Figure 5. Plot of Simbruini groundwaters in the ternary HCO_3^- -SO_4^{2-} -Cl^- a) and Ca^{2+} -Na^+-Mg^{2+} b) diagrams.
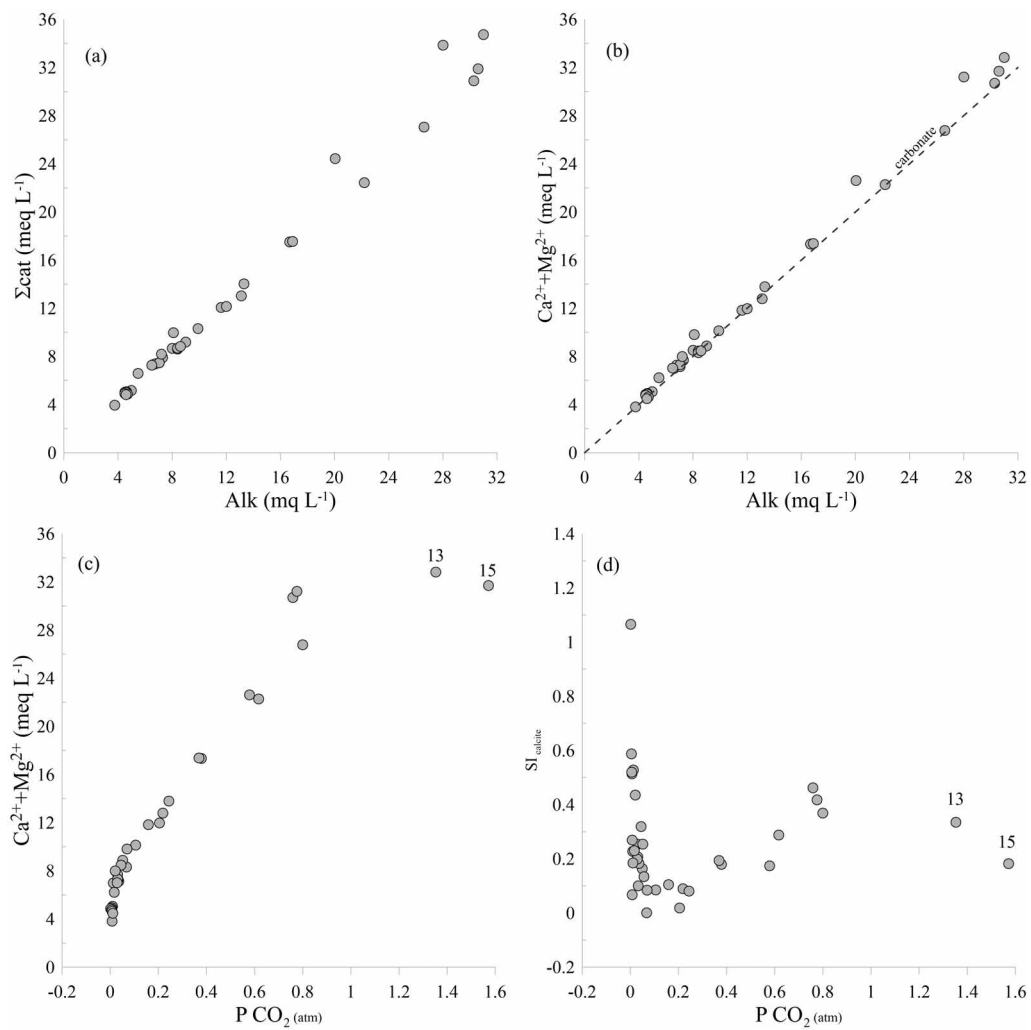

Figure 6. Binary chemical plots of Simbruini groundwaters. a) Alkalinity vs. Σcations; b) Alkalinity vs. Ca^{2+} +Mg^{2+}; c) PCO_2 vs. Ca^{2+} +Mg^{2+}; d) PCO_2 vs. SI.

Figure 7. Probability plots of HCO_3^- a), PCO_2 b), sum of cations (Σcat) c), and $Ca^{2+} +Mg^{2+}$ d), for the Simbruini groundwaters.

Id.	$\delta^{18}O$	δ^2H_{H2O}	$\delta^{13}C_{TDIC}$	$\delta^{13}C\ CO_2$	CH_4	CO_2	Eh
15	-9.4	-57	5.8	1.7	3.95E-02	775	37
17	-9.2	-56	7.4	2.6	7.41E-02	575	20
23	-8.6	-52	-6.0	-15.			-43.4
34	-8.3	-48	-13	-22	7.98E-05	7.6	-41.4
35	-7.9	-45	-12	-21	1.20E-04	5.0	-51
36	-9.2	-52	-12	-21		4.3	-42

Table 3. Oxygen, deuterium (‰ vs. V-SMOW) isotopic composition, carbon isotopic compositions of dissolved CO_2 (‰ vs. PDB), dissolved CH_4 and CO_2 contents (cc L^{-1} STP) and Eh (mV, measured in the field) of groundwater samples collected in 2019.
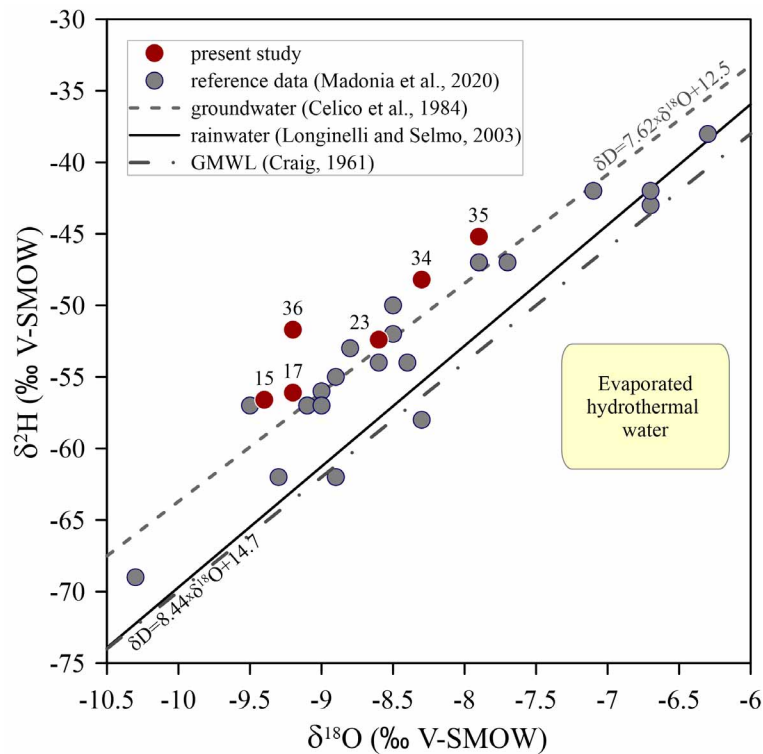
Figure 8. Plot of $\delta^{18}O$ vs δ^2H of samples collected in 2019. Reference data for other karst aquifer of Central Italy [Madonia, et al., 2020] are reported together with reference lines for groundwater [Celico, 1983] and for rainwater of Central Italy [Longinelli and Selmo, 2003], and the GMWL [Craig, 1961].

4.2 Inferences on groundwater circulation from chemical and isotopic data

The Langelier-Ludwig diagram (Figure 4) remarks that the samples fall in the bicarbonate alkaline-earth quadrant, as expected for karst water dominated by the dissolution of carbonate rocks, both limestones and dolostones, as remarked by the slight variability of Mg^{2+} concentrations (Figure 5b). In addition, a slight trend is observed toward a progressive enrichment in chlorine and sulphate. The ternary anion diagram (Figure 5a) indicates that this trend is driven by the delivery of sulphate, whose origin can be attributed to the interaction with sulfur gaseous species as H_2S. We excluded a possible chemical interaction with evaporitic deposits since these, as evidenced by the AGIP well Trevi 1, drilled in this area for hydrocarbon exploration, found evaporites at a depth of 2168 m b.w.h., too high for hypothesizing an involvement in the groundwater circulation system of Mts. Simbruini. [Dondi et al., 1966].

The SO_4^{2-} -richest samples are from the sites 1, 9-13, 15-17 and 21, and two of them (15 and 17) have also high dissolved CO_2 and CH_4 concentrations and calculated PCO_2. These sites are spatially clustered in the north-western corner of the studied area (Figure 1), suggesting the presence of tectonic discontinuities through which hydrothermal gases can migrate from depth interacting with the karst aquifers, as already suggested in previous studies [Percopo, 1998] and schematized in the hydrogeological profile of Figure 3.

This area is well defined in the PCO_2 map (Figure 9), where an anomaly is depicted by PCO_2 values exceeding 0.3 atm found in 8 sites. Another isolated, anomalous PCO_2 value has been recorded more to NW at the site 28 (an old roman-type dismissed well [Vinci, 1998]). Inferences on the origin of this CO_2 excess are given by the isotopic composition of total dissolved carbon (available only for 2019 samples). It is worth noting that the two samples with $PCO_2 > 0.3$ atm have a distinctly positive $\delta^{13}C$ (1.65 and 2.63 ‰, for samples 15 and 17, respectively), contrasting with the negative values (-15.49 to -22.15 ‰) of the samples with low PCO_2 (0.006 to 0.012 atm), typical of its organic origin, as expected in karst areas [Chiodini, et al., 1999]. The carbon isotopic composition of samples 15 and 17 is similar to that of the CO_2 discharged from the near Colli Albani quiescent volcano (Figure 1), which is considered of deep magmatic origin, being associated to a $^3He/^4He$ value of magmatic imprinting [Carapezza, et al., 2020].
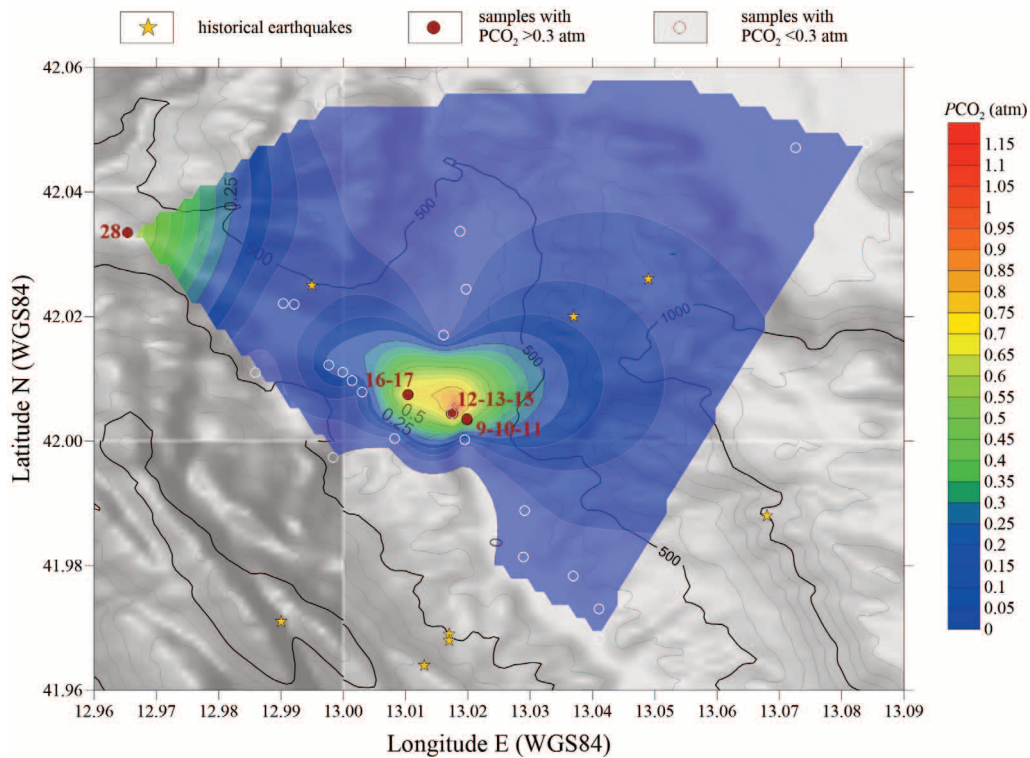
Figure 9. Map of dissolved PCO$_2$ and location of historical earthquakes (yellow stars) taken from the "Catalogo Parametrico dei Terremoti Italiani, versione CPTI15, [Rovida, et al., 2011]. Some low PCO$_2$ samples fall outside the SE limits of the map.

Chemical compositions of groundwater, concentrations of CH$_4$ and CO$_2$, and the isotopic signature of carbon dioxide are coherent in suggesting that, in a general scenario typical of a karst environment, there is a local anomaly due to the interaction with hydrothermal fluids rising from depth, mainly composed of non-organic CO$_2$, CH$_4$, and H$_2$S. Contrary to what observed as a general character of karst aquifers in Central Italy, where travertine deposits are often associated to deep CO$_2$ [Madonia, et al., 2020], travertine at spring 35 (Figure 10a) seems to be related to a simple loss of organic carbon dioxide. In fact, this spring shows low PCO$_2$ with an organic carbon isotopic signature. Conversely, a marked hydrothermal nature is found in site 17 (Figure 10b), a pool with flocculating sulphur and bubbling gases.

The isotopic signature of oxygen and deuterium of groundwater samples collected in 2019 further remarks the gaseous nature of the hydrothermal fluids interacting with the shallow, meteoric component of the aquifers, excluding a mixing with groundwater of deeper origin. In the δ^{18}O vs δ^2H diagram (Figure 8) the points related to the analysed samples occupy the same area of other reference values [Madonia, et al., 2020] for Central Italy, well fitted by the local groundwater line [Celico et al., 1984] but above the line representative of local rainfalls (LMWL) [Longinelli and Selmo, 2003].

A mixing with hydrothermal groundwater, richer in ^{18}O and ^{2}H, would shift the points in the lower right direction with respect the LMWL, e.g. toward the composition evidenced in yellow in Figure 8. Since we observe the opposite behaviour, a mixing between the meteoric recharge and deep, hydrothermal groundwater can be excluded. This fact is further remarked by the negative δ^{18}O values observed in springs no. 15 and 17, which are those with the best evidence of a chemical composition modified by a hydrothermal contribution. Their isotopic composition is quite similar to that one of spring no. 36, which receives a direct meteoric recharge from the highest elevated areas of Mts. Simbruini, as later discussed.

The oxygen isotopic signature of the collected groundwaters is helpful for reconstructing the residence time of the studied aquifers. In Figure 11, the elevation of the sampled sites is plotted against their δ^{18}O, together with two lines, both with slope of -0.0013 δ‰ m^{-1}, which represent the vertical variation of the yearly weighted average (intercept at -5.9 δ‰) and of the winter average (intercept at -8 δ‰) isotopic composition of rainfall for Central Italy [Longinelli and Selmo, 2003].
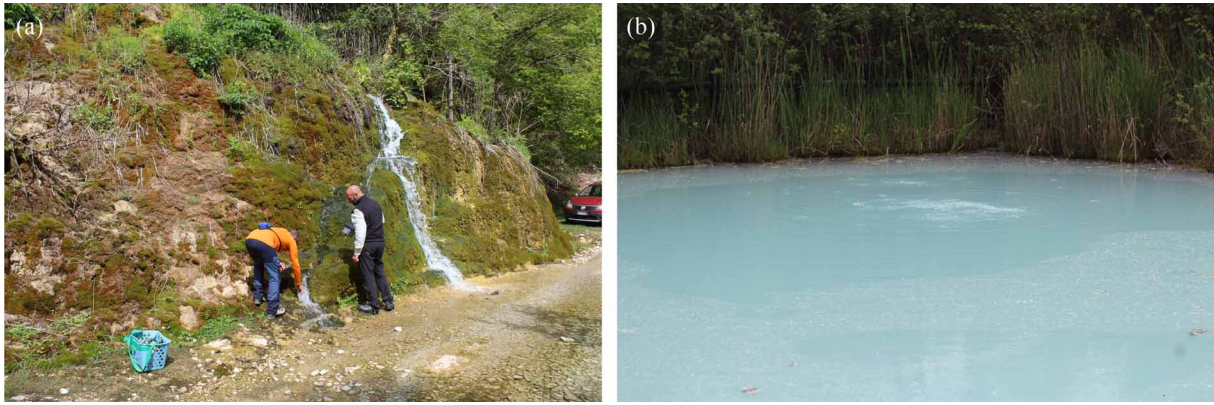
Figure 10. a) The Cardellino spring (site 35) forming a travertine deposit; b) the Lauriella pool (site 17) showing flocculating sulfur and bubbling gases.

Since the lowest point of an aquifer is its spilling point (spring), in the graph of Figure 11 a vertical line traced upward from the spring elevation should intersect the vertical isotopic gradient line in a point corresponding to the average elevation of the recharge area, inferred by the isotopic composition of rainfalls. This is true under the condition that the measured isotopic composition is equal to the yearly weighted average value of that spring.
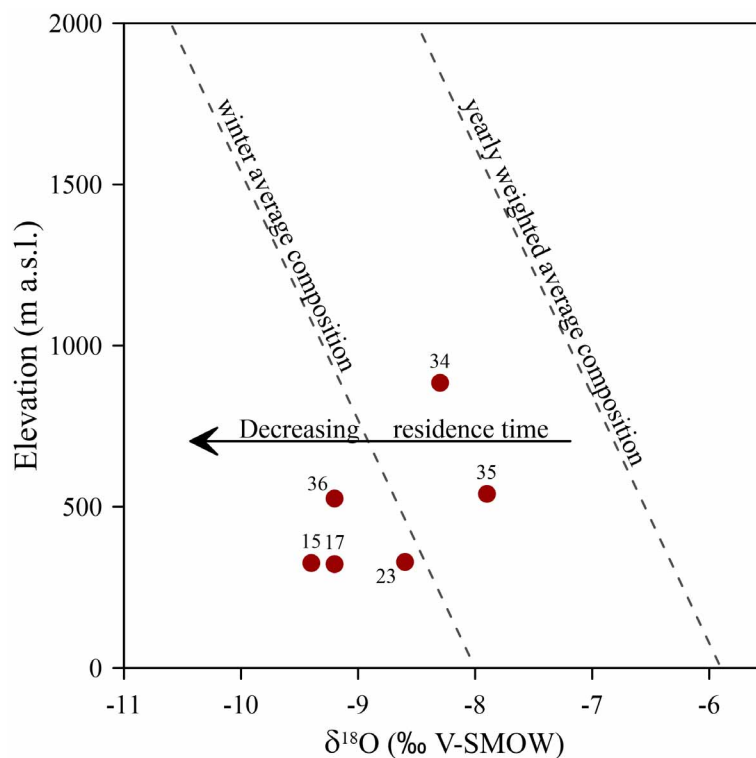
Figure 11. Plot of $\delta^{18}O$ vs elevation of 2019 groundwater samples, with vertical isotopic gradients for Central Italy (dashed lines) after [Longinelli and Selmo, 2003]. Two different gradients are represented: one calculated using the yearly average isotopic composition, weighted on rainfall amounts, and the other one using only winter precipitations.

As shown in the graph, only points 34 and 35 exhibit an isotopic composition compatible with this condition, whereas the positions of all the other points imply shorter residence times. In particular, the values measured in 15,

17, 23 and 36 suggest that at the time of sampling (May) the springs were releasing water infiltrated during the late autumn-winter months. A fast circulation, with mean residence times shorter than 1 year, is a typical feature of karst systems, where groundwater moves through wide conduits. This condition is remarked by field observations at site no. 36, a karst resurgence ("Inferniglio" spring) located at an elevation of 526 m a.s.l., draining a rock volume extended up to an altitude of 1550 m a.s.l. (Campo dell'Osso plateau), characterized by high mean flow rates (2.0 m^3 s^{-1}) modulated by huge variations following heavy showers. Small deposits of volcanic particles are found at this outlet, whose origin is the erosion and the following transportation as suspended solids of a thin (few tens of centimeters) pyroclastic level (alternations of volcanic sands rich in pyroxene phenocrysts and clayey ash) outcropping at Campo dell'Osso plateau. These deposits, found after flooding events, indicate that rainwater infiltrating at high elevations rapidly moves toward the basal aquifer through karst discontinuities, as large as to grant enough energy to maintain in suspension the volcanic particles.

Besides the Colli Albani volcanic complex, volcanic phenomena are reported in the area bordering the study zone, i.e. the two necks of Vicovaro and Mt. Autore to the north, and the lava effusions to the south-east [Accordi and Angelucci, 1962]. These findings confirm the existence of vertical discontinuities that favour either the hydrothermal fluid upraise and the rapid development of vertical karst conduits, which justify the short residence time of most of these waters.

5. Conclusions

The geochemical study carried out on 36 samples of Mts. Simbruini groundwaters, mostly from the Aniene valley, classifies these waters as bicarbonate alkaline-earth type hosted in a carbonate aquifer. The capture of these waters contributes significantly to the water supply of Rome city. The main process controlling the water chemical composition is water-rock interaction with dissolution driven by CO_2 of carbonates, as calcite, magnesium calcite and dolomite. Probability plots of HCO_3^-, $\sum$cations and $Ca^{2+}+Mg^{2+}$ indicate the presence of four water populations, the less represented of which (9 samples = 2 %) shows the highest PCO_2 values (> 0.3 atm). Most of the samples (8 out of 9) with anomalous content of dissolved CO_2 are from springs located in the central part of the study area, whereas the ninth is from an old well at the NW extremity of it (Figure 9).

The $\delta^{18}O$ isotopic composition of the water indicates, for most of the springs, a fast circulation typical of karst systems, with mean residence times shorter than 1 year.

A positive correlation between PCO_2 and $\delta^{13}C_{CO2}$ has been found in the six analyzed samples. Four samples have a very low PCO_2 (from 0.006 to 0.012 atm) and negative $\delta^{13}C_{CO2}$ (from -15.49 to -22.12 ‰ vs. PDB); two samples from the central area have distinctly higher PCO_2 (0.759 and 1.57 atm) and $\delta^{13}C_{CO2}$ values (1.65 and 2.63) similar to that of Colli Albani magmatic gas [Madonia, et al., 2020]. Therefore, geochemical data indicate that in the central part of the study area deep originated CO_2, uprising along fractures , fluxes the karst aquifer.

The absence of a ^{18}O isotopic shift in the analyzed samples suggests that there is no mixing between the meteoric recharge and deep hydrothermal groundwater, and that the hydrothermal contribution is limited to gaseous species of deep origin flushing shallow, meteoric aquifers.

References

Accordi, B. and A. Angelucci (1962). Un neck nel calcare cretacico di Monte Autore (Subiaco, Roma), Geologica Romana, 1, 289-296.

Andreas, W.H. and A. Hairigh (2008). ^{18}O-Equilibration on Water, Fruit Juice and Wine Using Thermo Scientific GasBench II. Thermo Fisher Scientific, Brema.

Cangemi, M., M.G. Di Figlia, R. Favara, and M. Liotta (2020). CO_2 degassing in Sicily (Central Mediterranean) as inferred from groundwater composition, Water, 12, 1959, doi:10.3390/w12071959.

Capasso, G., R. Favara, F. Grassa, S. Inguaggiato, and M. Longo (2005). On-line technique for preparing and measuring stable carbon isotope of total dissolved inorganic carbon in water samples ($\delta^{13}C$), Ann. Geophys., 48, 159–166.

Capasso, G. and S. Inguaggiato (1998). A simple method for the determination of dissolved gases in natural waters. An application to thermal waters from Vulcano Island, Appl. Geochem, 13, 631–642.

Capelli, G., L. Mastrolillo, R. Mazza, M. Petitta, T. Baldoni, F. Banzato D. Cascone, C. Di Salvo, and F. La Vigna (2012). Carta delle unità idrogeologiche della Regione Lazio, Foglio 2, 1:100.000.

Carapezza, M.L., M. Ranaldi, L. Tarchini, T. Ricci, and F. Barberi (2020). Origin and hazard of CO_2 and H_2S emissions in the Lavinio-Tor Caldara zone (Metropolitan City of Rome Capital, Italy), J. Volcanol. Geotherm. Res., 402, 106985, doi:https://doi.org/10.1016/j.jvolgeores.2020.106985.

Carminati, E., S. Fabbi and M. Santantonio (2014). Slab bending, syn-subduction normal faulting, and out-of-sequence thrusting in the Central Appennines, Tectonics, 33, 530-551; doi:10.1002/2013TC003386.

Célico, P., R. Gonfiantini, M. Koizumi, and F. Mangano (1984). Environmental isotope studies of limestone aquifers in central Italy, In Isotope Hydrology, IAEA: Vienna, Austria, 173–192.

Chiodini, G., F. Frondini, D.M. Kerrick, J. Rogie, F. Parello, L. Peruzzi, and A.R. Zanzari (1999). Quantification of deep CO_2 fluxes from Central Italy. Examples of carbon balance for regional aquifers and of soil diffuse degassing, Chem. Geol., 159, 205–222.

Craig, H. (1961). Isotopic variations in meteoric waters, Science, 133, 1702–1708.

Dondi, L.; Papetti, I. and Tedeschi, D (1966). Stratigrafia del pozzo Trevi 1 (Lazio), Geol. Rom., 5, 249-262.

Fabbi, S. (2016). Geology of the Northern Simbruini Mts. (Abruzzo – Italy), J. Maps, 12, 441-452, https://doi.org/10.1080/17445647.2016.1237899.

Kracht O. and A. Hilkert (2016). EA-IRMS: Fast and Precise Isotope Analysis of Liquids on a Delta V Isotope Ratio MS with a High Temperature Conversion Elemental Analyzer. Thermo Fisher Scientific, Brema.

Longinelli, A. and E. Selmo (2003). Isotopic composition of precipitation in Italy: a first overlap map, J. Hydrol., 270, 75–88.

Madonia, P., M. Cangemi, Y. Oliveri, and C. Germani (2020). Hydrogeochemical characters of karst aquifers in central Italy and relationship with neotectonics, Water, 12, 1926, doi:10.3390/w12071926.

Parkhurst, D.L. and C.A.J. Appelo (2020). Description of input and examples for PHREEQC version 3—A computer program for speciation, batch-reaction, one-dimensional transport, and inverse geochemical calculations: U.S. Geological Survey Techniques and Methods, http://pubs.usgs.gov/tm/06/a43 (accessed 12/02/2020).

Percopo, C. (1998). Idrogeologia del medio e alto fiume Aniene. PhD Thesis. Università degli studi di Roma "La Sapienza (In Italian), 101, https://www.idrogeologiaquantitativa.it/?p=2635&lang=it.

Rovida, A., R. Camassi, P. Gasperini, and M. Stucchi (2011). Catalogo parametrico dei terremoti italiani, versione CPTI11, Istituto Nazionale di Geofisica e Vulcanologia, Milano.

Sinclair, A.J. (1974). Selection of threshold values in geochemical data using probability graphs, J. Geochem. Explor., 3, 129–149.

Società Speleologica Italiana (2002). Carta delle principali aree e sorgenti carsiche d'Italia. Erga Edizioni, Firenze.

Stevanović, Z. (2015). Karst Aquifers – Characterization and Engineering, Springer, Cham, 687, doi:https://doi.org/10.1007/978-3-319-12850-4.

Stevanović, Z. I. Jemcov, and S. Milanovic (2007). Management of karst aquifers in Serbia for water supply, Environ. Geol., 51, 743–748, doi:10.1007/s00254-006-0393-z.

Vinci, M. (1998). Idrogeologia e Chimismo delle acque sotterranee del medio Aniene: anno di osservazione 1996, Thesis for Geological Science degree, La Sapienza University, Rome.

Zhang, J., P.D. Quay, and D.O. Wilbur (1995). Carbon isotope fractionation during gas-water exchange and dissolution of CO_2, Geoc. Cosm. Acta, 59, 107–114.

*CORRESPONDING AUTHOR: Massimo RANALDI,
Istituto Nazionale di Geofisica e Vulcanologia,
Roma, Italy,
e-mail: massimo.ranaldi@ingv.it